Thin sample refractive index by transmission spectroscopy

Michael Brindza,[1] Richard A. Flynn,[1] James S. Shirk,[2] and G. Beadie[1,*]

[1]*Optical Sciences Division, Naval Research Lab, 4555 Overlook Ave., SW, Washington, D.C. 20375, USA*
[2]*Sotera Defense Solutions, Inc., 7230 Lee DeForest Dr., Suite 100, Columbia, MD 21046, USA*
[*] *polymer_GRIN_lenses@nrl.navy.mil*

Abstract: Transmission spectroscopy and a small number of refractometer index measurements are combined to provide refractive index measurements of transparent samples ~50 um thick at hundreds of wavelengths with absolute accuracies $<1x10^{-4}$. Key to the technique is the use of independent index measurements to circumvent the need for an independent thickness measurement of the sample. The method was demonstrated on glass samples where fits to Cauchy curves had RMS accuracies $<3x10^{-5}$ from 415 to 1610 nm. Issues that must be addressed to reach this level of accuracy are discussed.

OCIS codes: (120.2650) Fringe analysis; (120.4530) Optical constants.

References and links

1. G. Beadie, J. S. Shirk, A. Rosenberg, P. A. Lane, E. Fleet, A. R. Kamdar, Y. Jin, M. Ponting, T. Kazmierczak, Y. Yang, A. Hiltner, and E. Baer, "Optical properties of a bio-inspired gradient refractive index polymer lens," Opt. Express **16**(15), 11540–11547 (2008).
2. Y. Jin, H. Tai, A. Hiltner, E. Baer, and J. S. Shirk, "New class of bioinspired lenses with a gradient refractive index," J. Appl. Polym. Sci. **103**(3), 1834–1841 (2007).
3. D. T. Moore, "Gradient-Index Optics: a Review," Appl. Opt. **19**(7), 1035–1038 (1980).
4. R. A. Flynn, E. F. Fleet, G. Beadie, and J. S. Shirk, "Achromatic GRIN singlet lens design," Opt. Express **21**(4), 4970–4978 (2013).
5. O. Cakmakci, "Optical design of a color-corrected 2.75 g visual loupe," Opt. Eng. **52**(11), 112–113 (2013).
6. P. Kotsidas, V. Modi, and J. M. Gordon, "Gradient-index lenses for near-ideal imaging and concentration with realistic materials," Opt. Express **19**(16), 15584–15595 (2011).
7. P. Kotsidas, V. Modi, and J. M. Gordon, "Realizable Planar Gradient-Index Solar Lenses," Opt. Lett. **37**(7), 1235–1237 (2012).
8. A. H. Ltd; Adam Hilger Ltd, "The Hilger-Chance Refractometer," J. Sci. Instrum. **25**(1), 18 (1948).
9. M. Born and E. Wolf, *Principles of Optics* (Pergammon Press, 1980), 6th ed., p. 323.
10. T. S. Moss, *Optical Properties of Semiconductors* (Butterworths Scientific Publications, 1959).
11. S. D. Poelman and P. F. Smet, "Methods for the determination of the optical constants of thin films from single transmission measurements: a critical review," J. Phys. D Appl. Phys. **36**(15), 1850–1857 (2003).
12. N. James, N. Hilfiker, T. Singh, D. Tiwald, S. Convey, S. M. Smith, J. H. Baker, and H. G. Tompkins, "Survey of methods to characterize thin absorbing films with spectroscopic ellipsometry," Thin Solid Films **516**(22), 7979–7989 (2008).
13. R. Ulrich and R. Torge, "Measurement of Thin Film Parameters with a Prism Coupler," Appl. Opt. **12**(12), 2901–2908 (1973).
14. Application Note "Bulk Material or Thick Film Index/Birefringence Measurement," Metricon Corporation, Pennington, New Jersey 08534.
15. N. J. Harrick, "Determination of Refractive Index and Film Thickness from Interference Fringes," Appl. Opt. **10**(10), 2344–2349 (1971).
16. S. H. Kim, S. H. Lee, J. I. Lim, and K. H. Kim, "Absolute refractive index measurement method over a broad wavelength region based on white-light interferometry," Appl. Opt. **49**(5), 910–914 (2010).
17. J. Ye, H. Jiao, Y. Su, and Z. Yang, "Simultaneous Measurement of Thickness and Refractive Index Based on Rotation Incidence Angle," J. Mod. Opt. **60**(11), 900–905 (2013).
18. B. E. A. Saleh and M. C. Teich, *Fundamentals of Photonics* (John Wiley & Sons, Inc., 1991).
19. C.-H. Tseng, J. F. Ford, C. K. Mann, and T. J. Vickers, "Wavelength calibration of a multichannel spectrometer," Appl. Spectrosc. **47**(11), 1808–1813 (1993).
20. S. T. Wollman, P. W. Bohn, S. T. Wollman, and P. W. Bohn, "Evaluation of Polynomial Fitting Functions for Use with CCD Arrays in Raman Spectroscopy," Appl. Spectrosc. **47**(1), 125–126 (1993).

#220152 - $15.00 USD Received 30 Jul 2014; revised 23 Oct 2014; accepted 27 Oct 2014; published 7 Nov 2014

21. R. C. Youngquist, S. M. Simmons, and A. M. Belanger, "Spectrometer wavelength calibration using spectrally resolved white-light interferometry," Opt. Lett. **35**(13), 2257–2259 (2010).
22. E. Perret, T. E. Balmer, and M. Heuberger, "Self-Consistent Algorithm for Calibrating Spectrometers to Picometer Accuracy over the Entire Wavelength Range," Appl. Spectrosc. **64**(10), 1139–1144 (2010).
23. K. Liu and F. Yu, "Accurate Wavelength Calibration Method using System Parameters for Grating Spectrometers," Opt. Eng. **52**(1), 013603 (2013).
24. I. H. Malitson, "Interspecimen Comparison of Refractive Index of Fused Silica," J. Opt. Soc. Am. **55**(10), 1205 (1965).
25. J. F. Offersgaard, "Waveguides formed by multiple layers of dielectric, semiconductor, or metallic media with optical loss and anisotropy," J. Opt. Soc. Am. A **12**(10), 2122–2128 (1995).
26. P. D. T. Huibers, "Models for the wavelength dependence of the index of refraction of water," Appl. Opt. **36**(16), 3785–3787 (1997).
27. J. M. Bennett and L. Mattson, *Introduction to Surface Roughness and Scattering,* 2nd ed. (Optical Society of America, Wash. D.C. 1999) Chap. 3.
28. A. Duparré, J. Ferre-Borrull, S. Gliech, G. Notni, J. Steinert, and J. M. Bennett, "Surface characterization techniques for determining the root-mean-square roughness and power spectral densities of optical components," Appl. Opt. **41**(1), 154–171 (2002).
29. M. Montecchi, R. A. Montereali, and E. Nichelatti, "Reflectance and transmittance of a slightly inhomogeneous thin film bounded by rough, unparallel interfaces," Thin Solid Films **396**(1-2), 264–273 (2001).

Introduction

Recently, a new class of polymer gradient refractive index (GRIN) materials was developed that allows the design of lenses with custom index variations within each element [1,2]. The potential for a custom index variation within an optical element adds new degrees of freedom for the design of GRIN optical devices [3]. These new materials can lead to novel designs for achromatic lenses [4,5] and to optics which cannot be easily fabricated from homogeneous optical materials [6,7].

Lens design requires accurate information on the refractive index across the entire wavelength range of interest. For bulk optical materials, techniques for the determination of refractive index and its dispersion with high accuracy are well known. Layered polymer GRIN materials present a case where available measurements are not sufficient. The fabrication of these new polymer GRIN lenses has been described [2]. In brief, a library of about 100 or so ~50 μm thick nanolayered films whose index values differ in steps of ~0.001 is produced. Selected films are stacked so that the refractive index varies across the stack in a manner defined by the desired lens gradient. Next, the stacks are consolidated, molded, cut and polished into an optical element. The index distribution and its dispersion in an element is determined by those of the component polymers, the order in which the films are stacked, the molding parameters for the consolidated stack, and the shaping of the final lens. An effective design requires accurate values for the refractive index and dispersion of the library of films. Effective fabrication requires not only index data, but also timely measurement of the hundreds of films stacked into each lens.

The desire for more accurate index and dispersion data on the polymer films from which the GRIN optics are fabricated motivated a search for a rapid, accurate method to determine their optical properties. The method should be simple and cheap enough to allow analysis during manufacturing. Specifically, the goal is measurement of the real part of the refractive index of ~50 um thick films at 200 or more wavelengths between 400 and 1600 nm with uncertainties better than ± $1x10^{-4}$ in an instrument suitable for laboratory or a manufacturing environment. The imaginary or absorptive part is assumed to be negligible for any useful bulk optical material. While that accuracy is attainable with currently available methods, those methods typically measure one wavelength at a time, which can be time consuming and create sparsely sampled dispersion curves.

The method described here is based on a spectrum of the many transmission fringes of a thin film, which can be rapidly acquired, combined with a few prism-coupler based refractometer measurements. To validate the method, experimental spectra of two different thickness BK7 glass samples and two different thickness fused silica samples are reported and

#220152 - $15.00 USD Received 30 Jul 2014; revised 23 Oct 2014; accepted 27 Oct 2014; published 7 Nov 2014

analyzed. The measured index is compared to literature and/or externally calibrated values at more than 200 wavelengths between 415 nm and 1610 nm. Results presented below reproduce the literature or reference dispersion curves with RMS accuracies better than $3x10^{-5}$.

The organization of the paper is as follows. In the first section, some background and the strategy of the technique is described. In the second, the spectroscopic instrumentation used to measure the interference fringes is described. The third section covers the details of how we convert fringe and refractometer data to retrieved dispersion curves, including our method of spectrometer calibration. The fourth section presents results from measurements of known reference materials, which validate the technique, followed by a conclusion section. The appendix presents details related to how systematic errors impact retrieved index errors, which motivate choices for experimental setup and analysis methods.

Technique

Among the methods used to measure refractive index of optical materials, the most accurate is to measure the angle of deviation of a laser passing through a precision prism made of the subject material [8]. The prism method measures the index of one wavelength at a time, and the tolerances on the prism fabrication and measurement are stringent. It is not applicable to the thin film materials here, since they cannot be fashioned into the required prisms.

There is an extensive literature on the determination of the refractive index of thin films [9–11]. The most common methods include Ellipsometry [12], prism coupling/refractometer measurements [13,14], and interference fringe measurements [15–17]. Refractometer measurements are usually the most accurate for the films of interest here, but since only one wavelength is measured at a time, it is inconvenient to measure a complete dispersion curve for many films. Here we describe how refractometry can be combined with the interference fringe spectrum to provide many accurate index measurements over a wide wavelength range.

For a thin, parallel sided film, transmission interference fringe maxima are given by [9]:

$$\lambda = (2 \cdot D) \cdot \frac{n(\lambda) \cdot \cos(\theta)}{M} \tag{1}$$

where D is the sample thickness, n is the wavelength-dependent index of refraction at the fringe maximum location for the fringe order M, λ is the fringe maximum wavelength, and θ is the internal, refracted angle within the sample. Poelman and Smet [11] review spectroscopic methods that have been used to determine the index values. The accuracy of refractive index values obtained with the reviewed fringe methods is typically on the order of 10^{-3}.

Here we combine independent refractometry with fringe spectra to determine both the sample thickness and fringe order, as measured by the spectrometer. With a commercial prism-coupler instrument, from Metricon, an index accuracy of ± $1x10^{-4}$ at a single wavelength can be achieved in the bulk refractometry mode. Averaging several measurements yields mean errors near 5 $x10^{-5}$. Knowing peak wavelengths λ from the fringe spectrum, our technique of solving for $n(\lambda)$ requires index measurements at two or more wavelengths to obtain independent determination of M and D. Once M and D are known, the index at each of the many other fringe peaks can be found using Eq. (1). While the experiment described below covers the visible and near-IR wavelengths, this is a general technique, capable of measuring refractive index of any transparent material over wide wavelength ranges.

Experimental apparatus

A schematic of the fringe spectrometer and its beam path is shown in Fig. 1. It was designed to provide both speed of acquisition and the simplicity necessary in a manufacturing environment.

#220152 - $15.00 USD Received 30 Jul 2014; revised 23 Oct 2014; accepted 27 Oct 2014; published 7 Nov 2014

Achieving the desired uncertainties in index requires sufficient wavelength resolution. Fringe spacing decreases at shorter wavelengths. In order to maintain a resolution greater than 1/10 of one fringe across the wavelength range 400 nm to 1600 nm, four static grating spectrometers are used, each with resolution consistent with the expected fringe spacing in the different wavelength regions. Two Ocean Optics model HR4000 were used to cover the wavelength ranges of 400-600 nm and 550-950 nm and two Ocean Optics model NIRQuest covered the 925-1300 nm and 1250-1625 nm ranges. The grating and slit width for each spectrometer was chosen such that the resolution at the shortest wavelength provided at least 10 pixels per fringe peak. Static spectrometers were chosen to minimize acquisition time and to enhance the calibration stability.

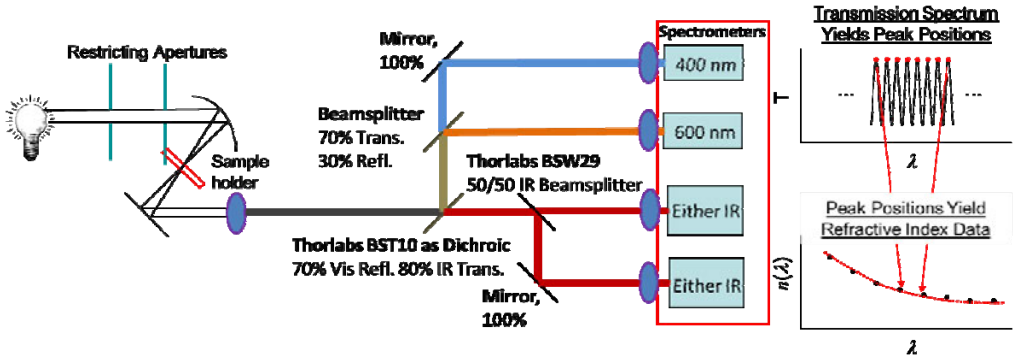

Fig. 1. Fringe spectrometer. White light transmitted through a thin sample is coupled into four static grating high resolution spectrometers by dichroic beam splitters and mirrors.

The white light source was a standard tungsten halogen source (Ocean Optics). A small analysis region is desirable to minimize the effect of film thickness variations, discussed in the Appendix. There is a trade-off between the spot size at the sample and the angular distribution of light, also discussed in the Appendix. To achieve this trade-off, light from the source is restricted by 2 mm apertures placed 16 inches apart and focused on the sample with a 50 mm focal length spherical mirror. This f/25 beam limits the spot size analyzed while also limiting the angle (θ) of off-axis rays. Despite the restricted aperture, the light source was sufficiently intense to give a spectrum acquisition time of less than 30 seconds.

Zemax simulations of the geometric spot size suggest the maximum extent of the beam in this configuration is roughly elliptical with outer dimensions ~600x300 um. Collimated on-axis light would focus to a round spot ~200 um in diameter. After the sample, the beam was recollimated and split into four beams. Collimating across the entire 400-1600 nm bandwidth is difficult. Zemax simulations showed that a 125 mm focal length BK7 singlet lens provides a good compromise for equal spot size at each spectrometer slit. The angular extent due to imperfect collimation into each slit is less critical for accuracy than at the sample, so long as the path into each spectrometer remains stable. Beamsplitting optics were chosen to maintain a high intensity in each path. Each beam was focused onto the appropriate spectrometer slit with a lens mounted on the spectrometer.

The fringes are recorded in the different spectral ranges by the four different spectrometers. In order to minimize differences in the area of the film surveyed by each spectrometer, two apertures (not shown in Fig. 1) after the sample select a common sample region that is probed by each spectrometer. This minimizes registration errors, but there is still a wavelength dependence of the spot size. An alternate method for collecting the spectra was attempted using an integrating sphere (Labsphere) to collect the light. However, in this configuration the optical signal was too weak, increasing the spectrum acquisition times unacceptably.

#220152 - $15.00 USD Received 30 Jul 2014; revised 23 Oct 2014; accepted 27 Oct 2014; published 7 Nov 2014

Refractive index calculations

The refractive index calculation combines a few Metricon measurements of $n(\lambda)$ at specific wavelengths with the fringe spectrum to determine absolute mode order numbers M and sample thickness D. Once D is known accurately, the index at each of the many fringe peaks is calculated from the wavelength value and mode order. For a non-uniform sample, as discussed in Appendix A, each spectrometer may see fringe peaks spaced according to different local thicknesses. The analysis below allows for this effective thickness variation, improving accuracy.

We distinguish here between two related values: M, integer fringe peak order, and script $\mathcal{M}$, accumulated optical path length in waves which can be a non-integer. The round trip optical path length, in waves, of normal incident light is

$$\mathcal{M} = \frac{2 \cdot n(\lambda) \cdot D}{\lambda} \tag{2}$$

which is similar to Eq. (1) but M need not be an integer. D can be found from measured Metricon (n, λ) pairs if the associated absolute $\mathcal{M}$ is known. Key to our approach is using the fringe spectrum, which generates (M, λ) pairs at each peak, as a "ruler" to measure the accumulated optical path, $\mathcal{M}$, that would occur at a given (n, λ) pair, measured separately by the Metricon, to high accuracy. Prior techniques have directly measured thickness. Our technique uses Metricon measurements to replace those direct thickness measurements.

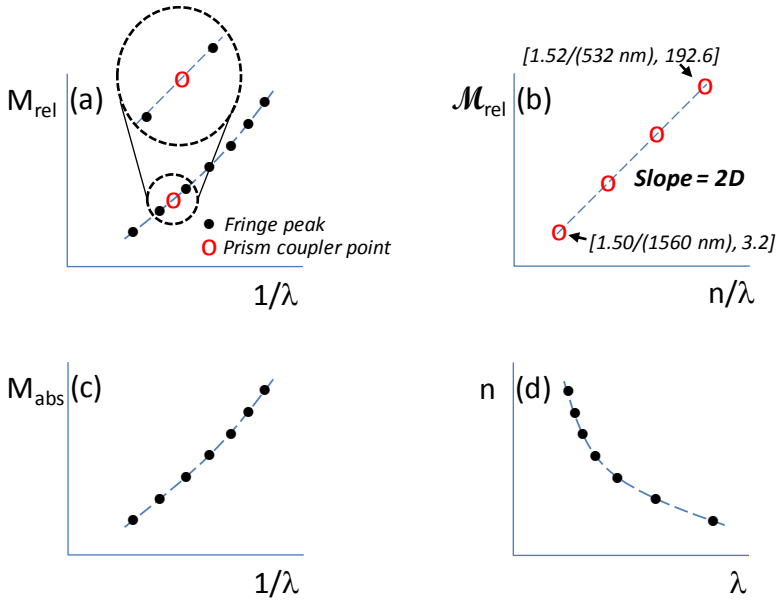

Fig. 2. How index values are found from Metricon measurements and fringe spectra. (a) Plot of M_{rel} vs $1/\lambda$ (black dots), the fringe peak "ruler," from which the relative optical path lengths $\mathcal{M}_{rel}$ of each Metricon (n, λ) pair are interpolated (red circles). (b) Sample thickness D is estimated by slope of Metricon $\mathcal{M}_{rel}$ vs n/λ. (c) Absolute mode order of fringe peaks M_{abs} is found from D and an (n, λ) pair. (d) Index data are calculated at each fringe peak from M_{abs} and λ, using the local thickness D per spectrometer. Peak and index values in (b) are representative of a 50 um thick BK7 sample. Actual fringe peaks are more closely spaced in λ.

Figure 2 illustrates how fringe peaks and Metricon (n, λ) pairs lead to a final dispersion curve. In Fig. 2(a), the relative accumulated optical path of each (n, λ) pair, relative to the first observed fringe peak, is interpolated between the nearest two fringe peaks. The accumulated

#220152 - $15.00 USD Received 30 Jul 2014; revised 23 Oct 2014; accepted 27 Oct 2014; published 7 Nov 2014

optical path is relative because the mode order of the first fringe peak is not yet known; this introduces the same constant offset in both M and $\mathcal{M}$. In performing the linear interpolation, we assume $n(\lambda)$ is constant between the two fringe peaks. As detailed in Appendix A, for our sample materials and geometry the uncertainty in approximating the optical path between two adjacent peaks with this assumption is $\sim 10^{-7}$, about two orders of magnitude below our current accuracy goal.

Next, the sample thickness D is estimated by plotting relative optical path versus $n(\lambda)/\lambda$ for the Metricon (n, λ) pairs, Fig. 2(b). Equation (2) dictates that this trend is linear, and that the slope, $2D$, is independent of the constant offset in $\mathcal{M}$ introduced by using relative optical path. This first estimate of D has some inaccuracy, due to the effective thickness variation with wavelength mentioned previously. However, with accurate enough spectrometer calibration, index measurement, and a sample with sufficiently plane parallel sides, the resulting thickness estimate is sufficient for the next step: finding absolute optical path and thereby absolute mode order of the fringes.

Figure 2(c) plots absolute mode order of the fringe peaks versus $1/\lambda$. The absolute mode order offset was found as follows. First calculate the absolute optical path of each (n, λ) pair, using D and Eq. (2), then subtract its relative optical path from Fig. 2(b). The difference, ideally, is the absolute mode order of the first fringe peak, e.g. the offset in M and $\mathcal{M}$. Some noise is present. A single value for the offset is found by averaging the result of all the (n, λ) pairs, and rounding to the nearest integer. The rounding inherent to assigning an integer offset compensates for inaccuracy in our first D estimate. Indeed, since our maximum mode order is typically ~300, even an accuracy as poor as 1/300 in the initial thickness estimate is sufficient to tell which integer label is the correct one. In practice the accuracy well exceeds 1/300 and the absolute mode order is strictly determined.

Finally, a dispersion curve is calculated, Fig. 2(d). Each fringe peak yields an individual sample of dispersion at its peak wavelength. Dispersion, $n(\lambda)$, is calculated from Eq. (1) using the wavelength and absolute mode order of each fringe peak and the thickness of the sample. In practice, greatest accuracy is attained by treating each spectrometer as having a different local sample thickness. A single Metricon (n, λ) pair situated near the center wavelength of each spectrometer is used to calculate the local sample thickness D through Eq. (2). This has the effect of "pinning" the dispersion curve at these Metricon values while the fringe peaks fill in the shape of the dispersion curve in-between.

Based on the approach detailed above, to reach our stated goal of overall index accuracies $<10^{-4}$, we need relative Metricon index uncertainties $<10^{-4}$ and relative wavelength uncertainties $<10^{-4}$. In the visible, for example, this implies a wavelength uncertainty near ± 0.02 nm. As already noted, we are able to average independent Metricon measurements to obtain index accuracies $<5\text{x}10^{-5}$. To obtain relative wavelength accuracies $<10^{-4}$, when spectrometer manufacturers typically specify only $\sim 10^{-3}$, required us to develop a detailed calibration procedure described in the following section. A more detailed discussion of several pertinent error sources is found in Appendix A.

In addition to optical constraints, the temperature of the spectrometer and sample must be controlled. For polymers, whose thermo-optic coefficient (dn/dT) can be $4\text{x}10^{-4}$/°C or larger, measuring with index accuracies of $5\text{x}10^{-5}$ requires sample temperature control on the order of 0.1°C. For the spectrometers, vendor data suggest temperature control on the order of 0.5-1.0 °C is required.

This technique is valid for thin, parallel sided, transparent materials. The thickness/refractive index combination must be in a range where fringes can be accurately observed. We have successfully measured 30 μm to 65 μm thick samples with an index near 1.5. Thinner samples are measureable to the same uncertainty, though they will have more sparsely spaced index data. Thicker samples are also possible, but the wavelength range covered would be limited by the spectrometer resolution at the blue end of the range.

#220152 - $15.00 USD Received 30 Jul 2014; revised 23 Oct 2014; accepted 27 Oct 2014; published 7 Nov 2014

Spectrometers with a resolution higher than those used here would be required. Optical materials are typically transparent and this technique was developed for non-absorbing samples. Index accuracy is maintained, however, in the presence of small absorption peaks. A simple Kramers-Kronig analysis [18] demonstrates that an absorption feature would have to be ~5 cm^{-1} or stronger to effect an index change $>10^{-5}$ in the visible spectrum.

Spectrometer calibration

Several approaches to the calibration of spectrometers with array detectors have been described in the literature. Often, a calibration is found by fitting a set of known atomic spectral lines to a polynomial [19,20]. In the miniature spectrometers used here both the dispersion and the instrumental line profile vary across the spectrometer's range. In this case, a reasonably dense set of calibration lines is required for calibrating the spectrometers to the desired uncertainty, to avoid an interpolation from distant calibration points. Interference fringes can provide closely-spaced calibration peaks in regions where good spectral lines are sparse. Youngquist et al. [21] used a Michelson interferometer to produce a set of lines at predictable wavelengths across the spectrum to produce a calibration with an error of ± 0.1 nm. Perret, Balmer, and Heuberger claimed picometer accuracy using an atomic calibration lamp combined with a Fabry–Perot etalon [22]. Their etalon gives sharp transmission lines over the full spectrometer range. An alternative strategy for calibration was used by Liu and Yu. They derived the calibration directly from the optical parameters of the spectrometer [23]. This is not practical for the miniature spectrometers here.

Each spectrometer in Fig. 1 was calibrated using the fringes from a fused silica glass etalon and lines from an Ar atomic lamp in concert. The etalon was ~50 μm thick and gave more than 200 interference fringe peaks across the four spectrometers. With appropriate exposure parameters we have used up to (27, 18, 8, and 11) Ar peaks per spectrometer, from the shortest to longest wavelength ranges, respectively. Fused silica was chosen in part because the literature suggests its dispersion curve is known and stable to the $1x10^{-5}$ level across multiple manufacturers [24].

Calibration was processed as follows. The mode order of each observed fringe was found as described in Fig. 2, where the known Ar lamp wavelengths and known index values of the reference etalon at those wavelengths take the place of the Metricon measurements. Uncertainty in the uncalibrated wavelength (the *x*-axis of Fig. 2(a)) is made up for by the plurality of Ar peaks at which the index is known. While the manufacturer's calibration is generally close enough to identify the correct mode order, Fig. 2(c), in cases where there is doubt one could begin with a raw spectrometer calibration based on the Ar line spectra, alone, before generating the Fig. 2(a) plot. With the mode order identified, each Ar line, with optical path length measured against the fringe peaks, provides a separate thickness estimate of the etalon, as per Eq. (2). In practice, the thicknesses extracted across a spectrometer vary by a small amount. A sample thickness is chosen for each spectrometer by averaging over all Ar line values observed on that array.

With a known thickness and a known dispersion curve for fused silica, each fringe peak provides a separate calibration point. Atomic lines provided between 8 and 25 additional calibration points per spectrometer. At the resolution desired, we found that the line shape in these spectrometers was wavelength dependent. A wavelength-dependent line-shape model was adopted for each spectrometer that empirically fit observed peak shapes. This was interpolated to find sub-pixel peak positions for each atomic line. The known wavelengths are compared to the measured wavelengths, and deviations are fit to a polynomial. We found that an eighth-order polynomial gave the desired accuracy, necessitated by several smoothly-varying minima and maxima in the measured wavelength residuals. While this is a high order calibration polynomial, it is well determined; the atomic lines and the fringes provided 30 to 100 calibration points per spectrometer.

#220152 - $15.00 USD Received 30 Jul 2014; revised 23 Oct 2014; accepted 27 Oct 2014; published 7 Nov 2014

The calibration procedure was accurate to relative wavelength values better than ± $3x10^{-5}$ over most of each spectrometer's range. It did approach ± $1x10^{-4}$ near the edges of a spectrometer's range in some cases, perhaps because the line shapes deteriorated there.

Verification: results and discussion

The accuracy of the method was tested on four inorganic glass samples with thicknesses in the target range. Two were BK7 etalons that were 38 μm and 67 μm thick, fabricated from the same batch of glass measured in Table 1, and two were fused silica, 52 μm and 55 μm thick.

The refractive index of the batch of BK7 used to fabricate the etalons was measured by the manufacturer with an uncertainty of ± $4x10^{-6}$ at the six wavelengths given in Table 1. The full dispersion curve was inferred by adding a small Lorentzian contribution, centered at a wavelength of 100 nm, to the nominal Schott BK7 curve. The peak location and amplitude of the Lorentzian perturbation were optimized to fit the data of Table 1. The final curve deviated from those data by no more than $1x10^{-6}$ at each wavelength.

Table 1. Schott reference material index data for our BK7 etalons; measured in air at 22.0°C.

Wavelength (nm)	BK7 index
435.84	1.526699
486.13	1.522388
546.07	1.518731
587.56	1.516809
656.27	1.514329

All our glass samples exhibited some degree of thickness variations across their surface as evidenced by a few dim fringes of color visible to the naked eye. The experimental uncertainty was reduced by acquiring fringe spectra from sample regions where the visual fringes are most uniform and widely spaced. Judging by the spacing of these fringes, of the four samples Fused Silica 1 had the least thickness variation over the largest area, so it was chosen as the calibration sample.

Sample spectra were acquired using the setup illustrated in Fig. 1. The glass samples were chosen to validate our technique because of their well-defined dispersion curves. The samples were too delicate to measure in the Metricon, so the analysis routines were provided with simulated Metricon measurements at four of the laser wavelengths available to our instrument: 473 nm, 780 nm, 1057 nm, and 1310 nm, selected so that each of the four spectrometers has a reference wavelength included. Simulated Metricon data points are given by fitting Eq. (3) to the index data provided by Schott glass (for BK7 samples) or Ref. 24 (fused silica samples), and inserting laser wavelengths. Since the data for BK7 has been provided, and Malitson shows evidence of index uniformity across many manufacturers of fused silica, we believe these simulated single wavelength index values are accurate to better than the desired $5x10^{-5}$.

Figure 3 shows the deviation of the raw index from the known index at each fringe peak, known either from the literature (fused silica) or from measurements by the manufacturer (BK7).

#220152 - $15.00 USD Received 30 Jul 2014; revised 23 Oct 2014; accepted 27 Oct 2014; published 7 Nov 2014

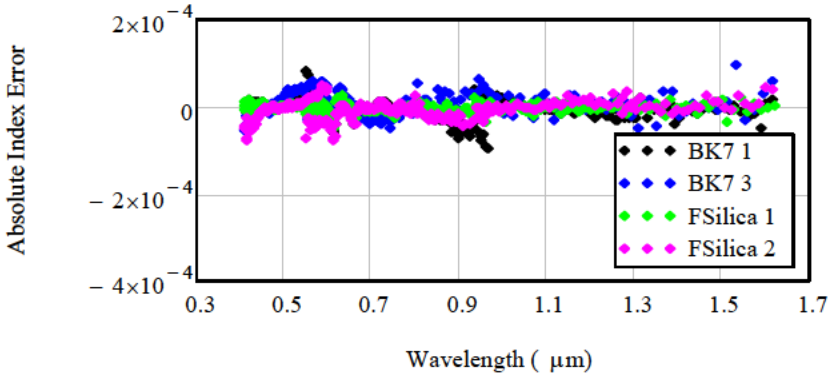

Fig. 3. Plot of representative set of raw refractive index errors for 4 different glass samples, after the system was calibrated using FSilica 1.

The data of Fig. 3 show random noise from peak to peak and systematic trends across each spectrometer (particularly at the shortest wavelengths.) Random error is attributed to the ability to identify sub-pixel fringe peak wavelengths in the presence of normal white noise in the spectrometer arrays.

The data points for each sample were fit to a 6 coefficient Cauchy function with the form:

$$n = \sqrt{v_0 + v_1\lambda^2 + \frac{v_2}{\lambda^2} + \frac{v_3}{\lambda^4} + \frac{v_4}{\lambda^6} + \frac{v_5}{\lambda^8}} \qquad (3)$$

The fits are shown in Fig. 4, with relevant quantities reported in Table 2.

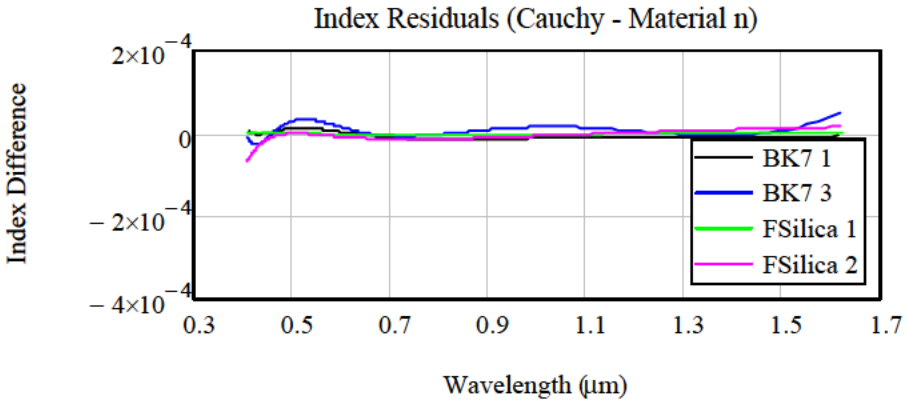

Fig. 4. Plot of Cauchy fits subtracted from reference curves for the index data used to generate Fig. 3. The RMS error in index was $<3\text{x}10^{-5}$, the maximum discrepancy was $< 1\text{x}10^{-4}$.

Of the various possible sources of systematic error, beyond inaccurate wavelength calibration, the ones explicitly considered as part of this work are evaluated in Appendix A. These include effects of sample tilt, surface film contamination, light focused too tightly onto the sample, and acquiring spectra through a region of non-uniform thickness. The apparent dominant source of systematic error in Fig. 3, based on the behavior of the data and the naked eye observation of colored fringes on the samples, is the effect of non-uniform thickness within the illuminated region of the samples. As demonstrated in the Appendix, thickness inhomogeneities effectively introduce an apparent, slowly varying thickness variation with

#220152 - $15.00 USD Received 30 Jul 2014; revised 23 Oct 2014; accepted 27 Oct 2014; published 7 Nov 2014

wavelength. By pinning this thickness value down at the four Metricon laser wavelengths, our index curves are led through the correct index value at each one, which bounds the systematic deviations in between.

Table 2. Thickness, minimum and maximum wavelength, number of peaks and Cauchy fit standard deviation (σ) of refractive index data generated from spectra of our etalons. Fused Silica 1, italicized, was used to calibrate the spectrometers.

Sample	Thickness (μm)	λ_{Min} (nm)	λ_{Max} (nm)	Number of Peaks	σ (raw)	σ (fit)
BK7 1	67	414	1614	417	$2.04x10^{-5}$	$8.73x10^{-6}$
BK7 3	38	411	1617	239	$2.55x10^{-5}$	$1.37x10^{-5}$
FSilica 1	*55*	*409*	*1621*	*334*	*$9.20x10^{-6}$*	*$2.37x10^{-6}$*
FSilica 2	53	410	1619	316	$2.25x10^{-5}$	$1.31x10^{-5}$

As can be seen from Table 2, index values were determined for at least 230 wavelengths for each sample. The standard deviation of the index errors was, in all cases, less than $3x10^{-5}$. The agreement between data and literature is greater for the Fused Silica 1 sample, because, as noted above, this data set was used to calibrate the spectrometers. When fit by a Cauchy curve, the fit values for the BK7 samples agreed with the manufacturer's measurements to within a standard deviation < $2x10^{-5}$. This agreement, particularly given that the spectrometers were calibrated with a sample of different material, provides strong evidence that the technique proposed in this paper, properly implemented, is capable of high accuracy index measurements over a broad wavelength range.

Conclusions

This paper presents a method of measuring the wavelength-dependent refractive index of thin samples by utilizing thin film interference effects observed in transmission spectra. Previous attempts were often limited in accuracy by the uncertainty in independently measured sample thickness. This work shows that independent measurements of sample thickness can be replaced by a few independent *index* measurements. When combined with transmission spectra, one can retrieve densely spaced dispersion curves from fringe peak positions with high accuracy.

We demonstrated RMS index accuracy better than ± $3x10^{-5}$ from 415 to 1615 nm for three glass samples, encompassing two different materials. This represents an improvement of more than an order of magnitude in accuracy over previously published interference-based techniques, to the best of our knowledge. In addition to improved accuracy, this technique provided several hundred index measurements over our wavelength range.

We also demonstrate an attractive calibration method for dispersive spectrometers, which utilizes the transmission spectrum of a known reference material and an atomic line spectrum. We demonstrated relative wavelength calibration accuracies better than ± $1x10^{-4}$ over all four of the spectrometers represented in Fig. 1, with accuracy better than ± $3x10^{-5}$ over most of the spectral range.

While our experiment relies on a custom arrangement of several high resolution static grating spectrometers, it is thought the method can extended into other wavelength ranges using different, scanning spectrometer technologies. The biggest difference for a scanning spectrometer will be establishing a calibration procedure with sufficient control over systematic wavelength errors.

APPENDIX A

Analysis approach

This Appendix will explore the effect of various systematic errors on retrieved index values. The analysis will be based upon variations of a model for the location of transmission fringe peaks. For a plane wave incident on a plane parallel sample with thickness *D* and dispersion

#220152 - $15.00 USD Received 30 Jul 2014; revised 23 Oct 2014; accepted 27 Oct 2014; published 7 Nov 2014

curve $n(\lambda)$ transmission peaks will be observed at a set of wavelengths $\{\lambda_M\}$ (curly braces meant to identify a set of values) where

$$\lambda_M = (2 \cdot D) \cdot \frac{n(\lambda_M) \cdot \cos(\theta)}{M} \tag{4}$$

and M values are integers, denoting the number of internal wavelengths per round trip (2 x D), and θ is the internal angle of propagation, relative to the sample surfaces. Rewritten in terms of the external angle θ_{ext} one can use Snell's Law to write:

$$\lambda_M = (2 \cdot D) \cdot \frac{\sqrt{n(\lambda_M)^2 - \sin^2(\theta_{ext})}}{M} \tag{5}$$

Rearranging terms to express index in terms of the other quantities, one obtains:

$$n(\lambda_M) = \sqrt{\left(\frac{M \cdot \lambda_M}{2 \cdot D}\right)^2 + \sin^2(\theta_{ext})} \tag{6}$$

Errors in the calculation of n arise from errors in the estimates of the wavelength, the thickness, and the external angle. It is assumed that measurements independent of the spectroscopy are accurate enough to determine the integer values of M precisely from the spectrum. It is assumed that Eq. (6) is used to calculate the set of estimated index values $\{n(\lambda_M)\}$ from experimental estimates $\{\lambda_M\}$, D, and θ_{ext}. It is assumed that each of these departs from their "true" values $\{\lambda^o_M\}$, D^o, and θ^o_{ext}. Thus, computed values of $\{n(\lambda_M)\}$ depart from their true values $\{n^o(\lambda_M)\}$ by an amount calculable from the dependence on the other parameters.

Uncertainties due to thickness

At normal incidence with a perfectly calibrated spectrometer, one finds:

$$n(\lambda_M) = \frac{M \cdot \lambda_M}{2 \cdot (D^o + \delta D)} = n^o(\lambda_M) \cdot \left(1 - \frac{\delta D}{D^o}\right) \tag{7}$$

Note that the error in calculating index with the wrong thickness is not constant: it scales with the index itself. For normally dispersive materials, this means the error gets worse in the blue end of the spectrum. To achieve a relative accuracy of 10^{-4} or better in index means being able to estimate D to a relative accuracy better than 10^{-4}.The errors introduced by thickness *variation* across a sample will be addressed separately.

Uncertainties due to angle

When incidence angle is the dominant error, one can write Eq. (6) as:

$$n(\lambda_M) = \sqrt{\left(\frac{M \cdot \lambda_M}{2 \cdot D^o}\right)^2 + \sin^2(\theta^o_{ext} + \delta\theta)} \tag{8}$$

In practice, one strives to achieve normal incidence, or $\theta_{ext} = 0°$. The leading order error in the estimate of the index is then:

$$n(\lambda_M) = n^o(\lambda_M) \cdot \left[1 + \frac{1}{2}\left(\frac{\delta\theta}{n^o(\lambda_M)}\right)^2\right] \tag{9}$$

Because the error in index is second order in the angle error, this suggests the angle requirements are not as strict as in some of the other quantities. This is true for collimated light, and a later analysis shows that tilt is, in practice, corrected for by a compensating

#220152 - $15.00 USD Received 30 Jul 2014; revised 23 Oct 2014; accepted 27 Oct 2014; published 7 Nov 2014

difference in sample thickness. In fact, the quadratic dependence has a deleterious effect in the presence of focused light. Focused light presents a distribution of incidence angles to the sample. Any deviation from normal incidence (left or right, top or bottom) has an additive impact on the index error. Simulations show that for light focused faster than f/20, data from our spectrometers would accumulate errors approaching 10^{-4} or greater due to this effect – even in the absence of other contributions to the error. As with the error due to thickness, the error due to sample tilt or tightly focused light is a nonlinear function of wavelength, in that it depends on $n(\lambda)$.

Uncertainties in estimated thickness

Sample thickness is estimated by interpolating independent index measurements between measured fringe peaks in a spectrum. As illustrated in Fig. 2, the estimated thickness is found from:

$$D \equiv \frac{1}{2n_m\kappa_m}\left(M_j + \frac{\kappa_m - \kappa_j}{\kappa_{j+1} - \kappa_j}\right) \tag{10}$$

where $\kappa_m = 1/\lambda_m$ is the wavenumber at a laser wavelength λ_m used in the measurement, n_m is the measured index, M_j is the peak order number of the peak just below κ_m, corresponding to wavenumber κ_j, and peak $(M_j + 1)$ is the peak just above at wavenumber κ_{j+1}. Assuming that the laser wavelength, and therefore κ_m, is known, uncertainties in the measured index and peak wavenumbers affect the relative uncertainty in the thickness according to:

$$\frac{\delta D}{D} \cong \sqrt{\left(\frac{\delta n_m}{n_m}\right)^2 + \left(\frac{\delta\kappa_j}{\kappa_j}\left(1-\Delta M\right)\right)^2 + \left(\frac{\delta\kappa_{j+1}}{\kappa_{j+1}}\Delta M\right)^2} \tag{11}$$

where ΔM is the fractional order number given by the second term in parenthesis in Eq. (10), and the analysis assumes $\Delta M/M << 1$ and $(n_{j+1} - n_j) << n_j$. For relative wavelength calibration uncertainty ~$3\text{x}10^{-5}$ and relative index measurement uncertainty ~$5\text{x}10^{-5}$ this predicts a relative uncertainty in the thickness of ~$7\text{x}10^{-5}$ in the thickness.

Even in the case of perfect information for n_m and the κ values, the thickness estimate would be in error for laser wavelengths that don't correspond to a fringe peak; the interpolation Eq. (10) is strictly valid only when the sample index does not vary between the two fringe peaks. The maximum error in the interpolation occurs when an index measurement wavenumber falls exactly between two peaks on the Fig. 2 plot, resulting in a relative thickness error given by (after an ancillary derivation, validated by direct numerical calculation):

$$\frac{\delta D}{D^o} = \frac{-\left(2n' + \kappa_m n''\right)}{32\left(D^o\right)^2\kappa_m n_m^3} \tag{12}$$

where n' and n'' denote first and second derivatives of the index function, respectively, with respect to wavenumber. In the derivation, the index is assumed to vary in the vicinity of κ_m according to:

$$n(\kappa) = n_m + \left(\kappa - \kappa_m\right)n' + \frac{1}{2}\left(\kappa - \kappa_m\right)^2 n'' \tag{13}$$

where the derivatives of the dispersion curve are evaluated at the measured wavenumber κ_m. For ~50 um thick samples of BK7, fused silica, or the polymers we intend to measure for gradient index lenses, one finds that the relative error $\delta D/D^o$ is ~10^{-7}. This is two orders of

#220152 - $15.00 USD Received 30 Jul 2014; revised 23 Oct 2014; accepted 27 Oct 2014; published 7 Nov 2014

magnitude below the accuracy we look to achieve, so we ignore any contribution to the error from our interpolation. For thinner samples, however, or more accurate measurements, this is an effect for which one might have to account.

How estimated thickness corrects for sample tilt

Because we estimate sample thickness from the data, errors in thickness and tilt angle are not independent. To second order a tilted sample presents itself as an untilted sample with a slightly different thickness. This relaxes the requirement on strict adherence to normal incidence, such that accurate dispersion measurements can still be made on flat samples tilted by a few degrees. To determine how estimated thickness compensates for small tilt angles to still generate accurate index values, recall that our measured thickness D is obtained from the interpolation process illustrated in Fig. 2. When the thickness is calculated under the assumption of normal incidence, it can be related to the true sample thickness when tilted by a nonzero thickness $\delta\theta$ via:

$$D = \frac{1}{2n_m\kappa_m}\left(2n_j\kappa_j D^o\sqrt{1-\frac{\sin^2(\delta\theta)}{n_j^2}}+\frac{\kappa_m-\kappa_j}{\kappa_{j+1}-\kappa_j}\right) \tag{14}$$

which is Eq. (10) with the expression for M_j expanded via Eq. (5) to show its dependence on tilt angle. When expanding this in line with the discussion surrounding Eqs. (10-12), we achieve:

$$D = D^o\left(1-\frac{1}{2n_m\kappa_m}\frac{\kappa_j\sin^2(\delta\theta)}{n_j}\right) = D^o\left(1-\frac{\lambda_m}{2n_m n_j\lambda_j}\delta\theta^2\right) \tag{15}$$

This is the value calculated as the thickness, when $\delta\theta$ is assumed to be zero but isn't. To see how this thickness error actually compensates for a calculation that ignores tilt angle, we compare the true index corresponding to peak number M_k

$$n^o(\lambda_k) = \sqrt{\left(\frac{M_k\cdot\lambda_k}{2\cdot D^o}\right)^2+\sin^2(\delta\theta)} \tag{16}$$

to the calculated index at that same peak

$$n(\lambda_k) = \frac{M_k\cdot\lambda_k}{2\cdot D} \tag{17}$$

(with Eq. (14) substituted into the denominator) to obtain:

$$n(\lambda_k)-n^o(\lambda_k) = n_k\frac{\delta\theta^2}{2}\left[\frac{\lambda_m}{n_m n_j\lambda_j}-\frac{1}{n_k^2}\right] \tag{18}$$

where n_k represents $n^o(\lambda_k)$ to zero-th order in $\delta\theta$. The bracketed quantity is generally very small because each of the two terms is nearly equal, being approximately the inverse of index squared. For typical polymers or glasses, the bracketed quantity is ~10^{-2}, meaning that the convolved error is one to two orders of magnitude less than the error in retrieved index from errors in either thickness (Eq. (14)) or tilt angle (Eq. (9)) alone, as evidenced by a direct comparison of the factors multiplying $\delta\theta^2$.From an experimental standpoint, simulations show that sub-10^{-4} accuracy can be obtained by assuming samples are normal to the incident light even if the actual angle is as high as 3-4°. The acceptable range of tilt angles would shrink if the sample index is higher. Equation (17) says the index error scales with index n_k, so if the sample index doubled the acceptable angular range would drop by a factor of two. The

#220152 - $15.00 USD Received 30 Jul 2014; revised 23 Oct 2014; accepted 27 Oct 2014; published 7 Nov 2014

comments from the previous section about the degree of collimation of that light, however, remain valid: the light must not be focused faster than ~*f*/20 should sub-10^{-4} accuracy be desired.

Uncertainties due to surface contamination

Retrieved index errors can be expected for samples with contaminated surfaces. We observed changes in the apparent dispersion curves of our etalons after sitting out in a laboratory environment over a period of months, which were eliminated by careful cleaning of the samples. To investigate the amount of contamination necessary to alter the fringe spectrum enough to distort recovered index values, a transfer matrix multilayer thin film code [25] was used to simulate the spectrum of an etalon coated with thin contaminant layers. Using water as a representative contaminant layer (Eq. (3) of Ref. 26) on samples of either BK7 or fused silica, it was determined that a layer thickness of only ~50 nm on each side of the sample was sufficient to generate retrieved index errors ~10^{-4}.

Uncertainties due to sample thickness inhomogeneity

The effect of sample thickness variations (roughness) on the transmission and reflection at optical surfaces has been studied extensively [27,28]. Montecchi et. al. [29] calculated the transmission spectrum of a thin film where each side of the film had a Gaussian distribution of roughness with an autocorrelation length greater than a wavelength but smaller than the area sampled. Their results showed that an increase in roughness caused a decrease in the fringe contrast but no systematic errors in the fringe peak positions.

In our experiments, we observed fringe peak location errors for high fringe contrast spectra. Asymmetry of the thickness distribution introduces inaccuracy into fringe peak positions, as detailed below. In our samples, the deviations about an average thickness are unlikely to have the symmetry of a Gaussian, especially when the spot illuminates only a portion of the overall sample. A model to include the effect of asymmetry in the thickness variation begins with imagining the illuminated region of the sample as subdivided into $j \in \{0...N\}$ elements, where each element corresponds to a plane parallel section of the sample with thickness D_j. The measured transmission spectrum of the sample is given by the normalized sum of each $j \in \{0...N\}$ transmission spectrum, computed for an etalon with a thickness of D_j, weighted by the local illumination spectrum. To be consistent with the expected slowly varying thickness for our samples, it is assumed that the thickness difference between neighboring areas is small.

Shown in Fig. 5 are sample geometries for two illustrative simulations. Fringe spectra are calculated for BK7 samples with a nominal thickness of 50 microns but differing amounts of wedge over a 2x2 mm^2 area, as indicated by the equations in the figure insets. The straight wedge could represent a region where the thickness is increasing uniformly in the area of the beam whereas the modified wedge might represent a region approaching a local peak in thickness.

#220152 - $15.00 USD Received 30 Jul 2014; revised 23 Oct 2014; accepted 27 Oct 2014; published 7 Nov 2014

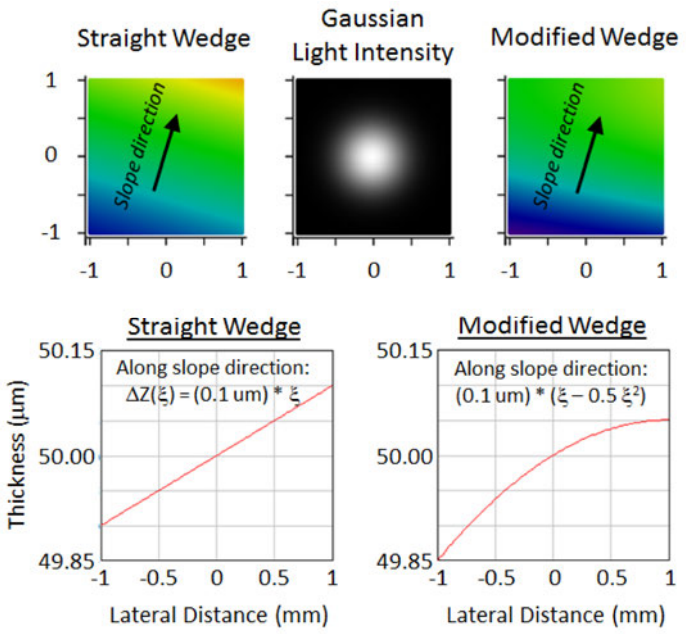

Fig. 5. Illustration of sample and illumination geometry for simulations of thickness effects on retrieved index data. The top contour plots show the topography of two wedged samples, plotted over a (2x2) mm^2 area. On the LHS the wedge is perfectly linear with a slope of 0.1 um/mm. On the RHS, the "wedge" is curved, according to the equation given in the inset. The illumination profile is Gaussian with a $1/e^2$ intensity half width of 0.6 mm (FWHM of 0.71 mm).

Sampling the geometries on a 301x301 grid, histograms of thicknesses weighted by the Gaussian light intensity are presented in Fig. 6. The histograms are very similar, in that they have the same peak to valley thickness difference and nearly the same FWHM. Both histograms are well fit by an asymmetric Gaussian distribution $exp[-(D-D_o)^2/\sigma^2]$ with a $1/e^2$ half width σ_L for all thicknesses $D_j < D_{pk}$ and σ_R for all thicknesses $D_j > D_{pk}$, where D_{pk} is the thickness at the peak of the distribution. The straight wedge histogram is perfectly symmetric, with a $1/e^2$ half width of 41 nm. The modified wedge histogram has values $(\sigma_L, \sigma_R) = (52, 25)$ nm.

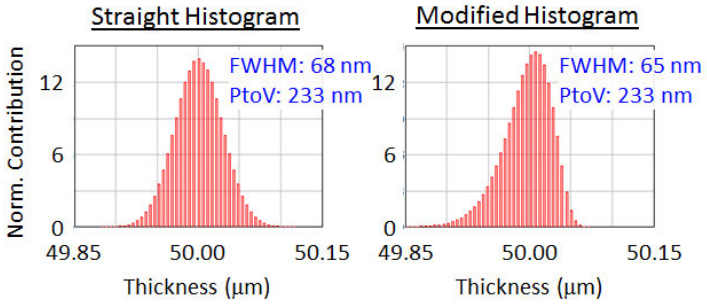

Fig. 6. Histograms of intensity-normalized thickness distributions from the sample geometries of Fig. 5. Histograms computed from numerical sampling of (2x2) mm^2 areas shown in Fig. 5, sampled across 301x301 points. The peak-to-valley thickness difference for each histogram is identical, at 233 nm.

We then simulate the fringe spectra which would be recorded in a measurement from each distribution and process these data to retrieve refractive index values from the fringe peaks.

#220152 - $15.00 USD Received 30 Jul 2014; revised 23 Oct 2014; accepted 27 Oct 2014; published 7 Nov 2014

Noise and wavelength calibration errors are added to the simulated data files to mimic our real spectrometer data files. We also simulated atomic lamp spectra and measured Metricon data. The batch of simulated data files was then processed using the same analysis code as used for the experimental data from elsewhere in the manuscript. The error between retrieved index values and the true index is shown in Fig. 7.

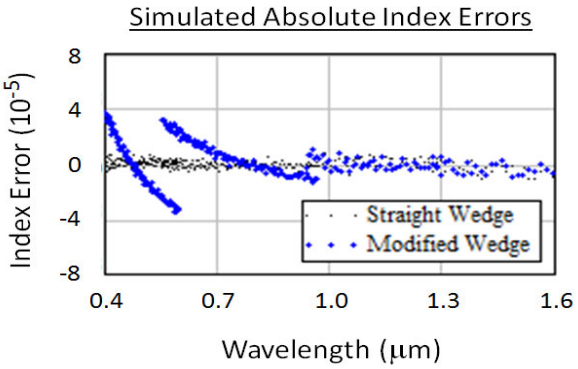

Fig. 7. Retrieved index errors from fringe spectra simulated with the histograms of Fig. 6, as approximated by asymmetric Gaussian functions and sampled at 101 evenly spaced intervals for each one. While the straight wedge allows for accurate index retrieval, the modified wedge results in fringe peak positions distorted across the spectra which result in systematic errors in recovered index.

The results in Fig. 7 highlight a crucial subtlety of the tolerance of the technique to thickness non-uniformity. Retrieved index values are sensitive to the *nature of the asymmetry* in the thickness variation and not just the *magnitude*. Samples with an asymmetric thickness variation can have systematic errors in the measured fringe maxima and hence in the retrieved index values. The model, which represents a typical thickness variation observed in our samples, shows that fringe errors are within our target of 1e-4 index accuracy. The shape and magnitude of retrieved index error will depend on the details the sample thickness distribution.

These systematic errors are equivalent to having a wavelength-dependent sample thickness in Eq. (1). The convolution of all the elements with different thickness results in a spectrum with fringe spacings that are not simply given by an average thickness. Note that similar effects would be seen with the perfect wedge if the light distribution was color-dependent. If, for example, red light preferentially illuminated the thinner part of the wedge then red wavelength fringes would exhibit a fringe spacing corresponding to thinner thicknesses than blue wavelengths.

The apparent discontinuities in the retrieved index at wavelengths where different spectrometers overlap arise because the spectra from different spectrometers are independently analyzed for sample thickness at a single Metricon wavelength. These wavelengths form the zero-crossings in Fig. 7. Were sample thickness evaluated at only a single wavelength, Fig. 7 would exhibit a continuous trend without discontinuity.

Acknowledgment

The authors wish to acknowledge DARPA for financial support for this work. The views expressed are those of the authors and do not reflect the official policy or position of the Department of Defense or the U.S. Government. Distribution Statement A: This document has been approved for public release, distribution is unlimited.

#220152 - $15.00 USD Received 30 Jul 2014; revised 23 Oct 2014; accepted 27 Oct 2014; published 7 Nov 2014